Microseismic source localization using time-domain path-integral migration[a]

[a]Published in SEG Expanded Abstracts, 2601-2606, (2016)

Yunzhi Shi[*1], *Dmitrii Merzlikin*[1], *and Sergey Fomel*[1]
[1]*The University of Texas at Austin*

ABSTRACT

Localization of passive seismic sources is crucial for real-time monitoring of hydraulic fracturing. Using the similarity of diffraction imaging and passive seismic imaging, we propose a method that uses path-integral formulation to apply diffraction-type migration on time-shifted microseismic records and to focus seismic energy focuses at correct onsets and accurate locations in time coordinates. An efficient workflow is applied to do path-integral migration based on analytical integration. Passive seismic sources can be additionally highlighted by envelope stacking. Numerical experiments with synthetic data verify the effectiveness of the proposed method.

INTRODUCTION

Microseismic monitoring is a technique that can provide real-time information about subsurface stimulated fracture networks. Microseismic data analysis involves passive seismic source localization (Maxwell, 2014). The traditional method is arrival-time inversion with traveltime picking adopted from global earthquake seismology (Warpinski et al., 1998; Gibowicz and Kijko, 2013). However, traveltimes can be difficult to pick (Duncan and Eisner, 2010). Alternative source localization methods without traveltime picking have been suggested, including the method described by Rentsch et al. (2007, 2010) and inspired by Gaussian-beam migration, time reversal imaging (Gajewski and Tessmer, 2005; Artman et al., 2010) and diffraction moveout stacking (Kao and Shan, 2004; Gajewski et al., 2007).

Conventional assumption for time-reversal microseismic localization is based on wave-equation imaging with densely sampled data and a known velocity. However, sparse downhole geophones and subjective velocity estimation both involve randomness which interferes with wavefield reconstruction and degrades the accuracy of source localizations (Sava, 2011). Complementarily, surface-sensor networks can be denser and more portable than borehole sensors, which resolves the problem of receivers sparsity; a surface network can be designed and optimized with the given aperture and fold requirements (Duncan and Eisner, 2010). Yet the surface network

is still sensitive to velocity errors under conventional depth imaging methods (Eisner et al., 2009).

As noted by Kao and Shan (2004) and Gajewski et al. (2007), passive seismic events can be focused by diffraction-type migration because of their similarity to diffractions in zero-offset sections. Migration applied on time-delayed data resembles reverse wavefield propagation, in which signals focus at source locations and true activating times. Microseismic monitoring can benefit from migration-based detection techniques that obtain a high value of the stack along the moveout curve, which overcomes the low signal-to-noise ratio (SNR) of the unstacked data (Chambers et al., 2010; Duncan and Eisner, 2010; Gharti et al., 2010; Bradford et al., 2013). Recently, Anikiev et al. (2013) and Staněk et al. (2015) suggested source mechanism correction combined with diffraction stacking in microseismic imaging.

Path-integral imaging provides an efficient way to image diffractions in time coordinates without velocity picking and produces a velocity independent image of the subsurface (Landa et al., 2006). Methodology of path-integral diffraction imaging (Burnett et al., 2011) is summation of a set of constant velocity images, generated by velocity continuation (Fomel, 2003b); in time domain, diffraction apices remain stationary whereas diffraction flanks change their shape. Stacking superimposes diffraction apices constructively and cancels flanks. An efficient workflow for path-integral imaging that combines velocity continuation and summation within analytical integration was recently proposed by Merzlikin and Fomel (2015). This method only requires a crude velocity range as a constraint instead of detailed velocity estimation. Furthermore, time-domain migration itself is not sensitive to prior velocity models (Fomel, 2014), and velocity analysis can be performed using double path-integral formulation (Schleicher and Costa, 2009; Merzlikin and Fomel, 2015).

In this paper, we propose to apply path-integral time-domain migration in a similar direct analytical way on microseismic data for imaging of passive sources. Prior estimation of the velocity model is not required. Instead, only a rough velocity range is necessary. The unknown activation times can be scanned since passive seismic energy will focus at true times and locations. This resembles the focusing of energy in back propagation wave process. We use synthetic data experiments to test the proposed method.

METHODOLOGY

In a microseismic data stream recorded by surface sensor networks, both excitation time and location of the source are unknown. An additional unknown factor, velocity, is involved and determined by estimation or prior information. Based on a specified velocity model, conventional imaging processes can be performed. In seismic diffraction imaging, path-integral time-domain migration (Burnett et al., 2011) bypasses velocity model construction and directly focuses hyperbolic events at source locations, if the onsets of the events are correctly compensated.

Efficient path-integral diffraction migration

Velocity continuation describes vertical and lateral shifts of time-migrated events under the change of migration velocity. The continuous process in a zero-offset isotropic case is described by equation (Claerbout, 1986; Fomel, 2003b):

$$\frac{\partial^2 P}{\partial t \partial v} + vt\frac{\partial^2 P}{\partial x^2} = 0. \tag{1}$$

Applying double-Fourier transform after time warpping $\sigma = t^2$, the solution for equation 1 can be expressed as (Fomel, 2003a):

$$\tilde{P}(k, \Omega, v) = \tilde{P}_0(k, \Omega) e^{\frac{-ik^2v^2}{16\Omega}}, \tag{2}$$

where v is migration velocity, Ω is the Fourier dual of σ and k is wavenumber. The input zero-offset stack $\tilde{P}_0(k, \Omega)$ is transformed to a constant velocity time migrated image $\tilde{P}(k, \Omega, v)$. Burnett and Fomel (2011) provide an extension to the 3-D anisotropic case.

The path-integral formulation creates velocity independent images (Landa et al., 2006) in time domain; the formulation of velocity-weighted path-integral of VC images is:

$$I(t, x) = \int_{v_a}^{v_b} W(v) P(t, x, v)\, \mathrm{d}v, \tag{3}$$

where $W(v)$ is the velocity-weighting function used to fine-tune velocity constraints formed by v_a and v_b.

Efficient workflow of the integral above, proposed by Merzlikin and Fomel (2015), is integrating velocity analytically in the double-Fourier domain. For example, an unweighted integral takes the form:

$$\begin{aligned} \tilde{I}(k, \Omega) &= \tilde{P}_0(k, \Omega) \int_{v_a}^{v_b} e^{\frac{-ik^2v^2}{16\Omega}}\, \mathrm{d}v \\ &= \tilde{P}_0(k, \Omega) e^{i\frac{5\pi}{4}} \frac{2\sqrt{\Omega\pi}}{k}\, \mathrm{erfi}(e^{i\frac{3\pi}{4}} \frac{kv}{4\sqrt{\Omega}}) \Big|_{v_a}^{v_b}, \end{aligned} \tag{4}$$

which turns path-integral into an analytical filter in double-Fourier domain. Velocity-weighting function with analytical forms can be included also in this integral.

The efficient path-integral time migration workflow for passive seismic data imaging can be summarized as:

1. Apply different time shifts τ to passive seismic data to cancel onsets; all operations afterwards are done for each constant τ slice.
2. Apply $\sigma = t^2$ time warpping to t-x-τ domain data.
3. Double-FFT transform from σ-x-τ domain to Ω-k-τ domain.

4. Apply equation 4 to build the filter in the double-Fourier domain.
5. Apply the filter in last step to Ω-k-τ data.
6. Inverse FFT and inverse time warpping into t-x-τ image.

Because the path-integral filtering is implemented in Ω-k-τ domain independently without data communication, all computations can be performed efficiently and in parallel.

Imaging condition: envelope stacking

In microseismic imaging, the objects of imaging are source locations. Recently, Sun et al. (2015) and Nakata and Beroza (2016) proposed a cross-correlation imaging condition for time reverse microseismic imaging; Trojanowski and Eisner (2016) reviewed imaging conditions based on diffraction stacking method, including envelope stacking imaging condition suggested by Gharti et al. (2010).

In the proposed workflow, we first extend passive seismic data $D(t, x)$ into a shifted domain $D(t, x, \tau)$, in which τ represents the source onset time:

$$D(t, x, \tau) = D(t + \tau, x). \tag{5}$$

For each τ slice of $D(t, x, \tau)$, we apply diffraction imaging to image passive seismic events, resulting in image $I(t_0, x_0, \tau)$.

In the image volume $I(t_0, x_0, \tau)$ created by path-integral time-domain migration, we apply envelope stacking along τ axis so that sources can be highlighted at their true location in time coordinates. Phase information is not discarded in this case because migration is applied before envelope stacking. Additionally, we apply a Laplacian sharpening operator in the image domain after envelope stacking to emphasize the maxima for easier visual picking.

After spatial localization of passive seismic sources, each time-delay trace is extracted from image volume $I(t_0, x_0, \tau)$ at position (t_0, x_0), showing the activation time of each source.

NUMERICAL EXAMPLES

Our first synthetic example consists of four isolated passive seismic events in a constant velocity (1.5km/s) media, shown in Figure 1 The sources are activated at 0.5s, 0.6s, 0.8s and 0.9s, from left to right. Amplitudes of the sources increase from left to right. Note that the 2nd source (0.6s) and 3rd source (0.8s) are aligned at the same depth in the model, they appear shifted in the seismic recording because of their activation time lag.

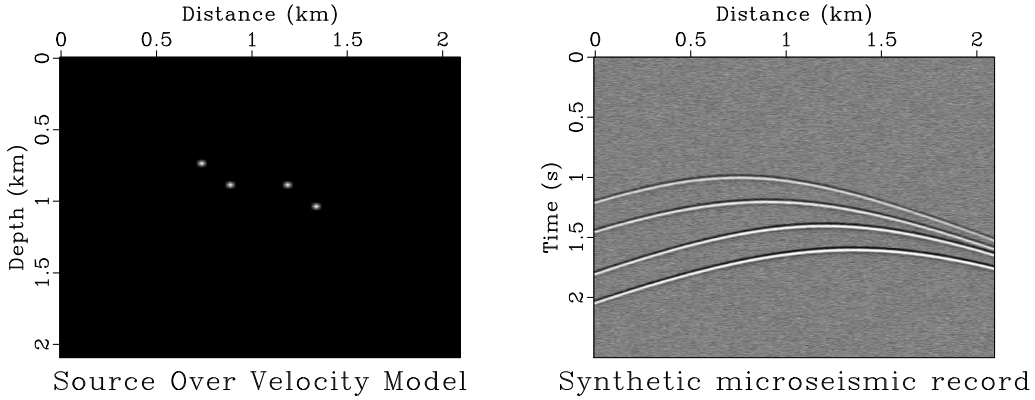

Figure 1: Synthetic microseismic model (left) and forward modeling data (right). Sources are activated at 0.5s, 0.6s, 0.8s, 0.9s,respectively from left to right. Amplitudes of the sources increase from left to right. simple/ data-simple

Figure 2 shows the construction of reverse-shifted hypercube. Data is sprayed to an extended dimension—reverse-time shift, then shifted along the time axis and padded after recording time. The time shift compensates for activation time lag of the passive seismic events. Migration can be performed on each t-x slice of this data hypercube.

After processing with proposed path-integral time-domain diffraction imaging on the extended dataset $D(t, x, \tau)$, some slices of the image volume $I(t_0, x_0, \tau)$ are shown in Figure 3. The path-integral migration only requires velocity limits (maximum and minimum values of velocity) instead of detailed velocity model estimation; for this constant velocity model, we add 0.3km/s of velocity uncertainty in the migration. At the delay times corresponding to the true activation times (0.5s, 0.6s and 0.8s), the sources focus at their true locations; at other incorrect activation time (0.7s), no event focuses.

Using amplitude envelope stacking, Laplacian sharpening and then converting to depth coordinates, a stacking image of source localizations is shown in Figure 4 with comparison between the true model and time-domain migration image. Although noise contaminates localization image, the four sources are easy to identify as a clear pattern. The spatial localizations match the sources locations in the synthetic model.

In the image in Figure 4, we can pick four sources' spatial locations; another task is to determine their activation times. Extracting the time-shift traces from image volume $I(t_0, x_0, \tau)$ at four picked sources positions, the traces are shown in Figure 5. From the upper to the lower part, the wavelets in the trace indicates onsets of the corresponding source. The temporal activation times match the onsets in the model.

Our next example includes a more complicated velocity model, cropped from

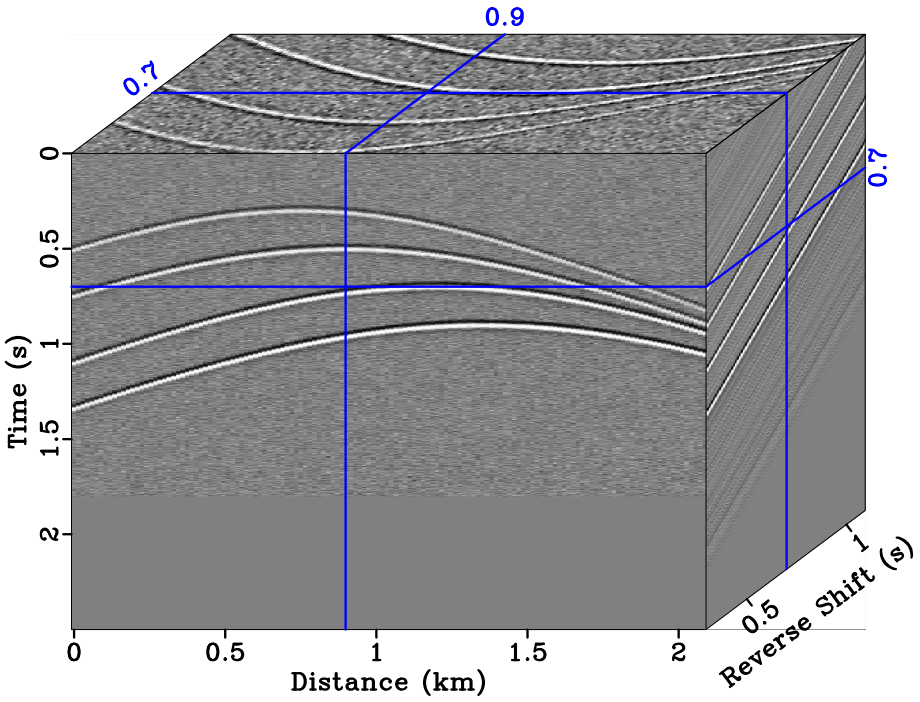

Figure 2: Shifted data hypercube. Data is sprayed on another reverse-shift dimension, then shifted on each slice corresponding to the reverse-shift value. simple/ shift

the Marmousi model (Versteeg, 1994) to test the stability of the proposed time-migration method in the presence of velocity heterogenities. Figure 6 demonstrates this synthetic model. The sources are divided into three groups, activated from left to right, resembling the three stages of fracture growth in hydraulic fracturing.

Instead of stacking along all reverse-shift values, stacking can also be performed within a sliding time window that includes certain stages of the injection. Figure 7 is the stacking image within the first, second, third stage and the full range of injection, respectively. We applied thresholding after envelope stacking and converted time-coordinate images to depth coordinates using the same velocity model for comparison. Microseismic events activated at the corresponding stage are focused, while other events that are not activated in this stage are defocused and suppressed after envelope stacking. Stacking image over full range shows all three stages of sources.

Figure 8 shows the stacking image over full range of stages superimposed on the velocity model.

DISCUSSION

Our examples considered microseismic sources as impulsive compressional sources similar to subsurface scatteres that generate diffractions. As noted by Anikiev et al. (2013) and Staněk et al. (2015), microseismic sources are mostly shear sources that

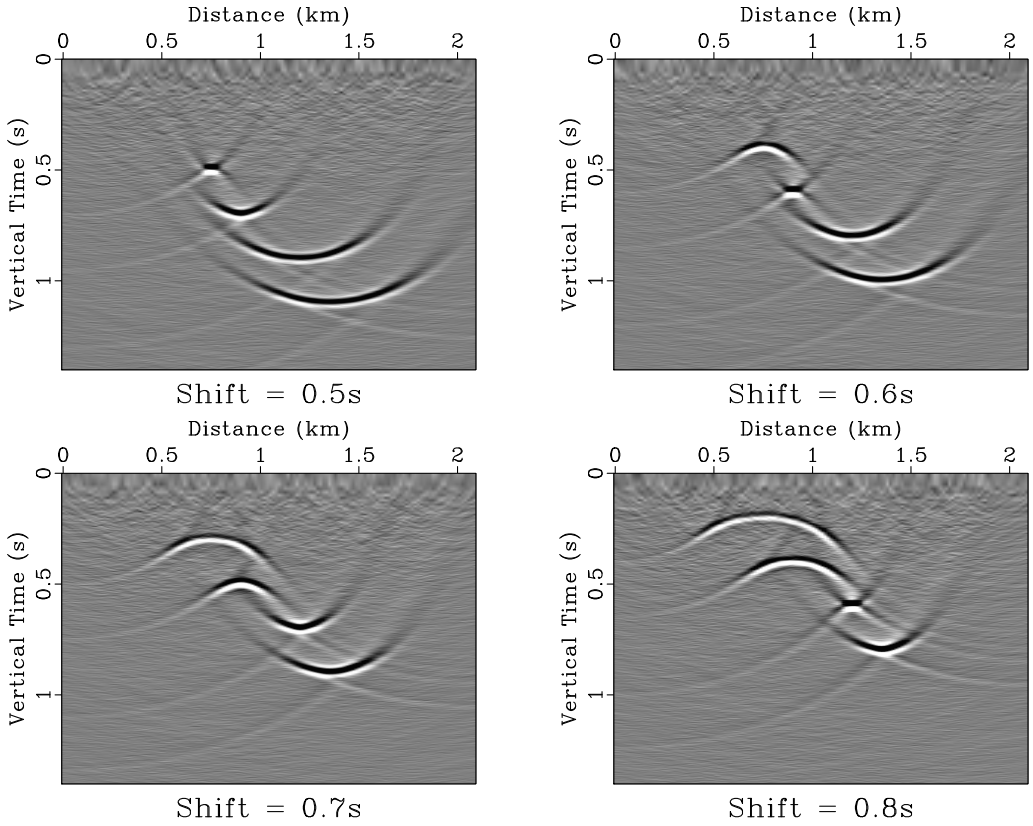

Figure 3: Passive seismic energy focus, corresponding to their true on sets, at their locations. simple/ act

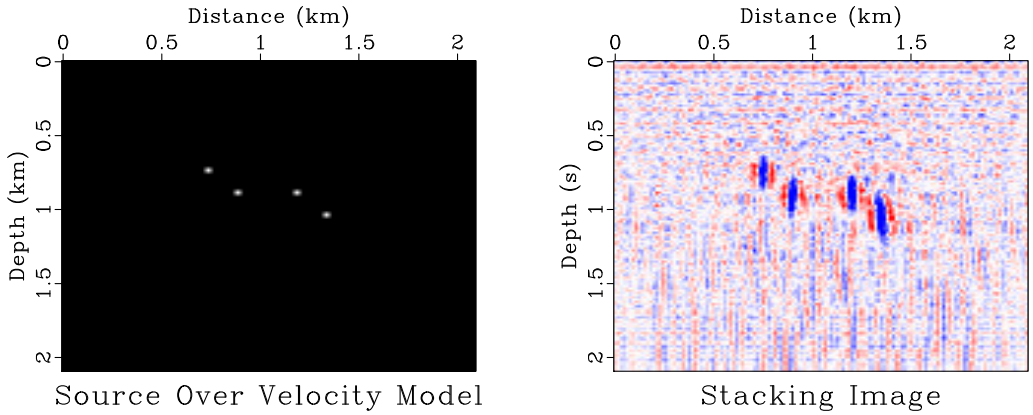

Figure 4: Microseismic imaging result of first synthetic example. Comparison between (left) synthetic model and (right) microseismic imaging after envelope stacking and Laplacian sharpening. simple/ migstack-simple

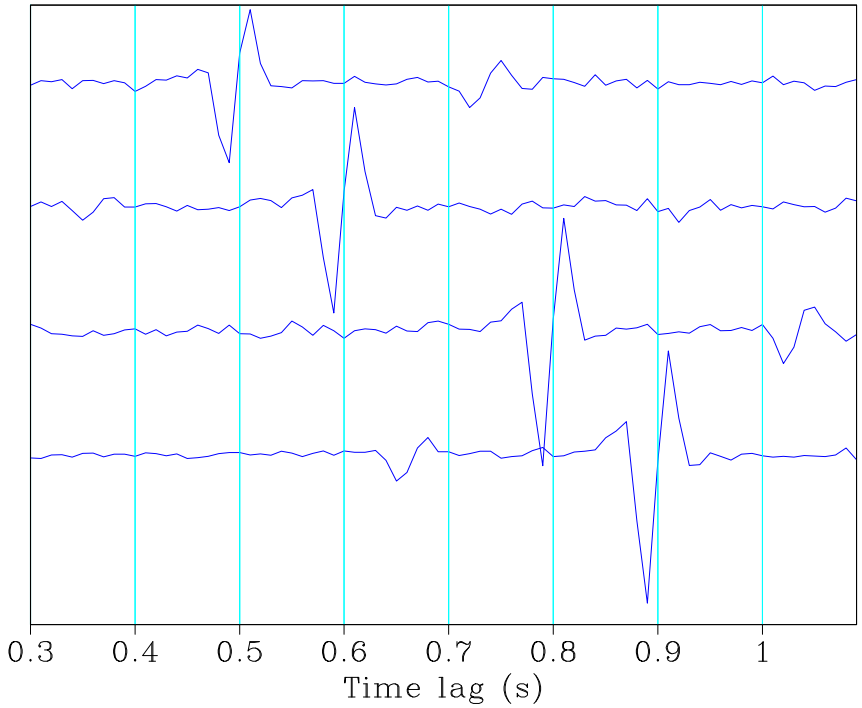

Figure 5: Four traces extracted from image volume $I(t_0, x_0, \tau)$ at four picked source positions. simple/ trc

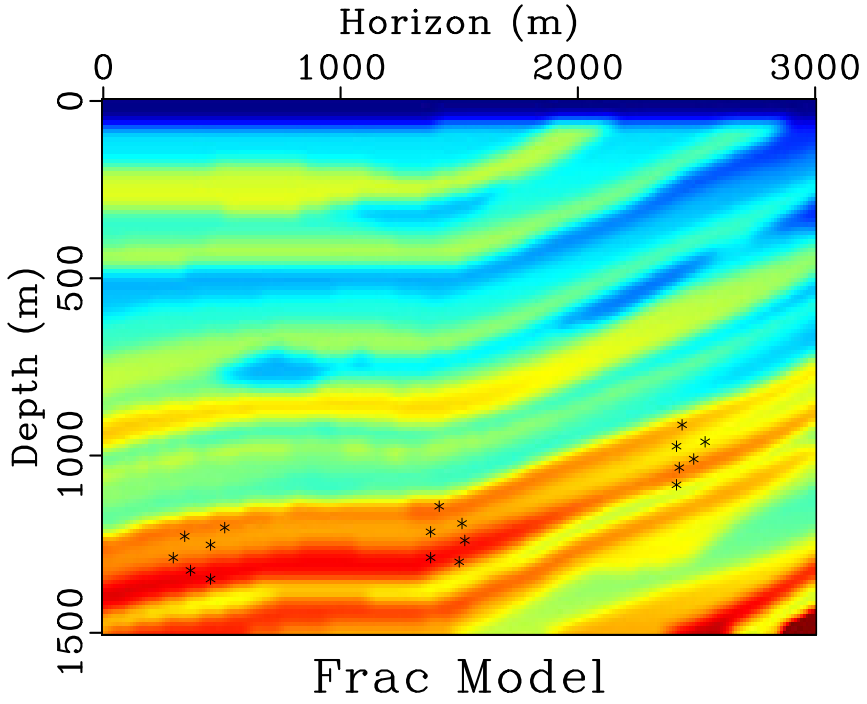

Figure 6: Source locations over velocity model. Three groups subsurface microseismic sources are activated from left to right. This is similar to the three stages of fracture system growth in hydraulic fracturing. marm/ sov

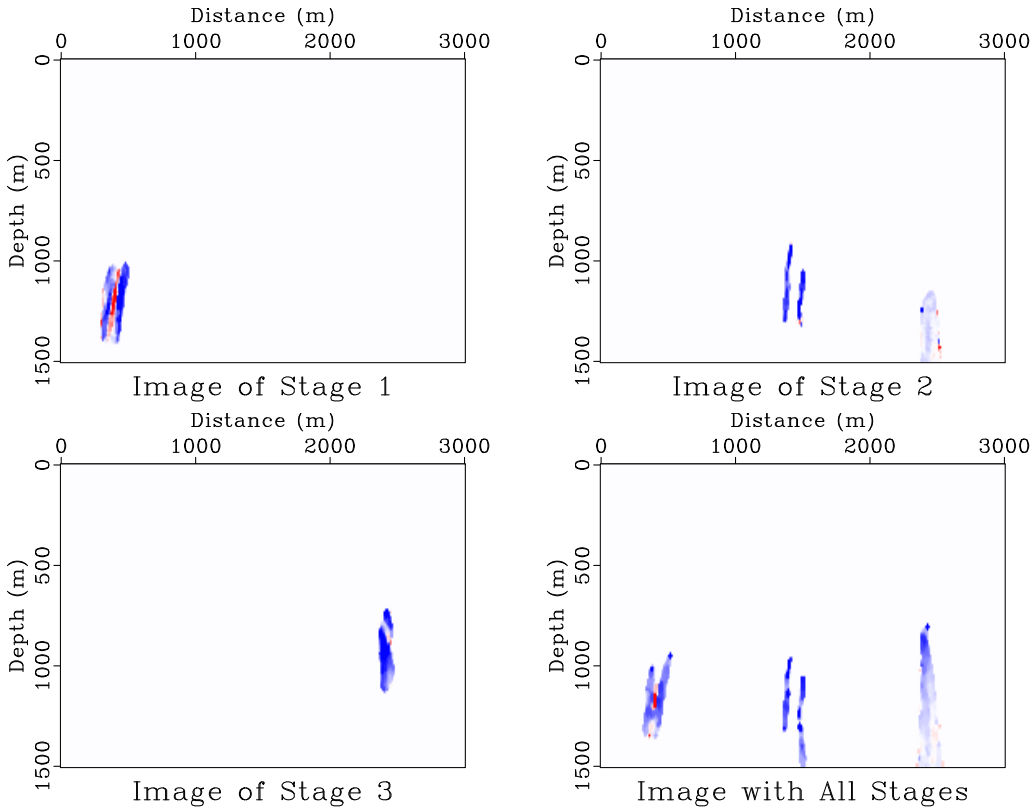

Figure 7: Stacking images over first, second and third stage of injection and full range of reverse-time shifting. marm/ migstack

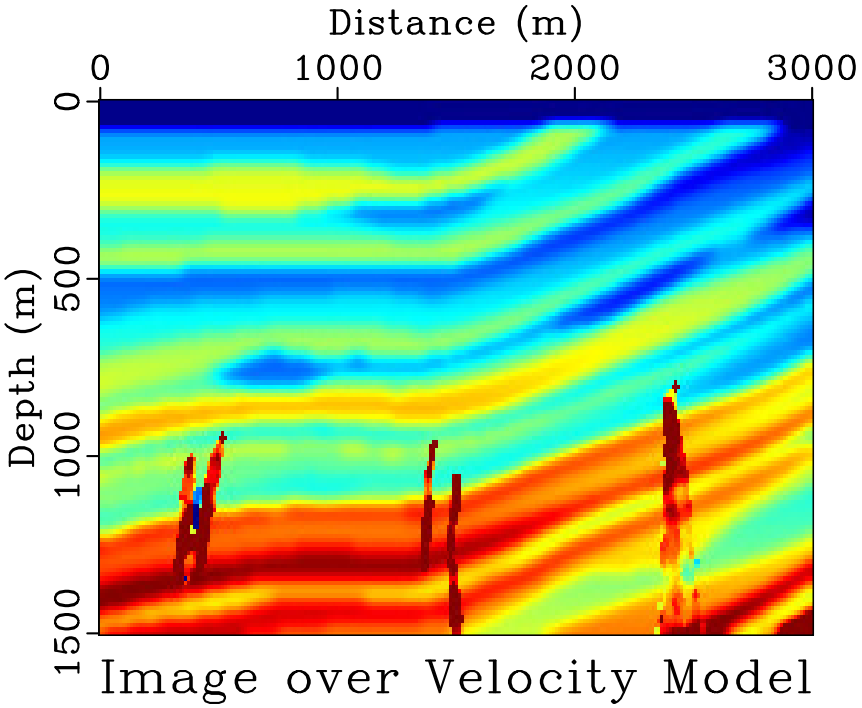

Figure 8: Microseismic imaging with full range of stages, superimposed on velocity model. marm/ mig-vel

have different radiation patterns. For example, the stacking value along moveout curve of a double-couple source event is ideally zero. Therefore, a radiation pattern correction for the source mechanism should be taken into account in diffraction imaging applied to passive data.

Conversion from time coordinates to depth coordinates after time-domain imaging is necessary and requires time-domain velocity analysis. Velocity analysis can be performed along with the migration process, by using the double path-integral formulation (Schleicher and Costa, 2009; Merzlikin and Fomel, 2015). Recent advances in time-domain seismic imaging bring other possibilities, including velocity-independent imaging using local slopes (Fomel, 2007; Cooke et al., 2009) and time-to-depth conversion in the presence of lateral-velocity variations (Cameron et al., 2008; Li and Fomel, 2015).

CONCLUSIONS

Microseismic source localization can be improved by migration-type diffraction imaging methods that stack passive seismic events along the moveout curves.

Compared to depth migration, diffraction-type time-domain migration is less sensitive to the subsurface velocity model. Path-integral migration can focus microseis-

mic events in time-domain efficiently using only crude velocity limits. It can also serve as a tool for providing velocity information.

By spraying seismic data into a time-reverse shift hypercube, migration is performed on each slice of the shifted data and results in a time-shifted migration image that resembles the propagation of microseismic wavefield. By stacking the envelope along time-reverse shift axis, energies are focused at sources locations in the time-domain image. Our synthetic examples show that the proposed method can be stable in the presence of random noise and velocity heterogenities.

ACKNOWLEDGMENTS

We thank Junzhe Sun and Tieyuan Zhu for helpful discussions and TCCS sponsors for financial support.

REFERENCES

Anikiev, D., F. Staněk, J. Valenta, and L. Eisner, 2013, Imaging microseismic events by diffraction stacking with moment tensor inversion: 83rd Annual International Meeting, SEG, Expanded Abstracts, 2013–2018.

Artman, B., I. Podladtchikov, and B. Witten, 2010, Source location using time-reverse imaging: Geophysical Prospecting, **58**, 861–873.

Bradford, I., T. Probert, D. Raymer, A. Ozbek, P. Primiero, E. Kragh, J. Drew, and C. Woerpel, 2013, Application of coalescence microseismic mapping to hydraulic fracture monitoring conducted using a surface array: Presented at the 75th EAGE Conference. (http://dx.doi.org/10.3997/2214-4609.20131028).

Burnett, W., and S. Fomel, 2011, Azimuthally anisotropic 3D velocity continuation: International Journal of Geophysics, **2011**. (http://dx.doi.org/10.1155/2011/484653).

Burnett, W., S. Fomel, and R. Bansal, 2011, Diffraction velocity analysis by path-integral seismic imaging: 81st Annual International Meeting, SEG, Expanded Abstracts, 3893–3902.

Cameron, M., S. Fomel, and J. Sethian, 2008, Time-to-depth conversion and seismic velocity estimation using time-migration velocity: Geophysics, **73**, VE205–VE210.

Chambers, K., J. Kendall, S. Brandsberg-Dahl, and J. Rueda, 2010, Testing the ability of surface arrays to monitor microseismic activity: Geophysical Prospecting, **58**, 821–830.

Claerbout, J. F., 1986, Velocity extrapolation by cascaded 15 degree migration, *in* SEP-48: Stanford Exploration Project, **79**, 84.

Cooke, D., A. Bóna, and B. Hansen, 2009, Simultaneous time imaging, velocity estimation, and multiple suppression using local event slopes: Geophysics, **74**, WCA65–WCA73.

Duncan, P., and L. Eisner, 2010, Reservoir characterization using surface microseismic monitoring: Geophysics, **75**, A139–A146.

Eisner, L., P. M. Duncan, W. M. Heigl, and W. R. Keller, 2009, Uncertainties in passive seismic monitoring: The Leading Edge, **28**, 648–655.

Fomel, S., 2003a, Time-migration velocity analysis by velocity continuation: Geophysics, **68**, 1662–1672.

———, 2003b, Velocity continuation and the anatomy of residual prestack time migration: Geophysics, **68**, 1650–1661.

———, 2007, Velocity-independent time-domain seismic imaging using local event slopes: Geophysics, **72**, S139–S147.

———, 2014, Recent advances in time-domain seismic imaging: 84th Annual International Meeting, SEG, Expanded Abstracts, 4400–4404.

Gajewski, D., D. Anikiev, B. Kashtan, E. Tessmer, and C. Vanelle, 2007, Localization of seismic events by diffraction stacking: 77th Annual International Meeting, SEG, Expanded Abstracts, 1287–1291.

Gajewski, D., and E. Tessmer, 2005, Reverse modelling for seismic event characterization: Geophysical Journal International, **163**, 276–284.

Gharti, H. N., V. Oye, M. Roth, and D. Kühn, 2010, Automated microearthquake

location using envelope stacking and robust global optimization: Geophysics, **75**, MA27–MA46.

Gibowicz, S. J., and A. Kijko, 2013, An introduction to mining seismology: Elsevier.

Kao, H., and S.-J. Shan, 2004, The source-scanning algorithm: Mapping the distribution of seismic sources in time and space: Geophysical Journal International, **157**, 589–594.

Landa, E., S. Fomel, and T. Moser, 2006, Path-integral seismic imaging: Geophysical Prospecting, **54**, 491–503.

Li, S., and S. Fomel, 2015, A robust approach to time-to-depth conversion in the presence of lateral-velocity variations: Geophysical Prospecting, **63**, 315–337.

Maxwell, S., 2014, Microseismic imaging of hydraulic fracturing: Society of Exploration Geophysicists.

Merzlikin, D., and S. Fomel, 2015, An efficient workflow for path-integral imaging of seismic diffractions: 85th Annual International Meeting, SEG, Expanded Abstracts, 4096–4100.

Nakata, N., and G. C. Beroza, 2016, Reverse time migration for microseismic sources using the geometric mean as an imaging condition: Geophysics, **81**, KS51–KS60.

Rentsch, S., S. Buske, S. Gutjahr, J. Kummerow, and S. Shapiro, 2010, Migration-based location of seismicity recorded with an array installed in the main hole of the San Andreas Fault Observatory at Depth (SAFOD): Geophysical Journal International, **182**, 477–492.

Rentsch, S., S. Buske, S. Lüth, and S. Shapiro, 2007, Fast location of seismicity: A migration-type approach with application to hydraulic-fracturing data: Geophysics, **72**, S33–S40.

Sava, P., 2011, Micro-earthquake monitoring with sparsely sampled data: Journal of Petroleum Exploration and Production Technology, **1**, 43–49.

Schleicher, J., and J. C. Costa, 2009, Migration velocity analysis by double path-integral migration: Geophysics, **74**, WCA225–WCA231.

Staněk, F., D. Anikiev, J. Valenta, and L. Eisner, 2015, Semblance for microseismic event detection: Geophysical Journal International, **201**, 1362–1369.

Sun, J., T. Zhu, S. Fomel, and W.-Z. Song, 2015, Investigating the possibility of locating microseismic sources using distributed sensor networks: 85th Annual International Meeting, SEG, Expanded Abstracts, 2485–2490.

Trojanowski, J., and L. Eisner, 2016, Comparison of migration-based location and detection methods for microseismic events: Geophysical Prospecting. (http://dx.doi.org/10.1111/1365-2478.12366).

Versteeg, R., 1994, The marmousi experience: Velocity model determination on a synthetic complex data set: The Leading Edge, **13**, 927–936.

Warpinski, N., P. Branagan, R. Peterson, S. Wolhart, and J. Uhl, 1998, Mapping hydraulic fracture growth and geometry using microseismic events detected by a wireline retrievable accelerometer array: Presented at the SPE Gas Technology Symposium. (http://dx.doi.org/10.2118/40014-MS).